D and *E* region incoherent scatter radar density measurements over Jicamarca

Jorge L. Chau and Ronald F. Woodman
Radio Observatorio de Jicamarca, Instituto Geofísico del Perú Lima, Perú

Received 20 September 2005; revised 19 October 2005; accepted 25 October 2005; published 29 December 2005.

[1] We present the first daytime *E* and *D* region incoherent scatter radar (ISR) measurements of electron densities at equatorial latitudes, using the Jicamarca ISR. Both measurements have been obtained using a high-resolution ISR mode with a relatively short interpulse period. Usually, *E* region ISR measurements are not feasible due to the clutter caused by strong echoes from equatorial electrojet irregularities (EEJ). Our *E* region ISR measurements were possible during an event when EEJ echoes were absent and show an excellent agreement with an empirical model based on rockets measurements (FIRI). In addition, we show that the employed high resolution mode also works to get densities between 130 and 200 km even during strong EEJ events, a region that is poorly known. In the case of *D* region densities, normally they are difficult to obtain due to the presence of strong coherent echoes caused by mesospheric turbulent layers. Fortunately, these layers are usually organized in narrow regions; therefore using a high range resolution, we have been able to get weak signals from the regions in between the layers causing coherent echoes. Our preliminary results show that our *D* region density estimates are in reasonable agreement with empirical models, in some cases providing slightly larger values. These new *D* region estimates contain important geophysical information that we plan to explore in the future.

Citation: Chau, J. L., and R. F. Woodman (2005), *D* and *E* region incoherent scatter radar density measurements over Jicamarca, *J. Geophys. Res.*, *110*, A12314, doi:10.1029/2005JA011438.

1. Introduction

[2] In this work we report the first daytime Incoherent Scatter Radar (ISR) measurements of electron densities from regions previously not accessible by ISR techniques at equatorial latitudes, i.e., the *E* and the *D* region. The importance of these measurements can be appreciated if we consider that the electron densities from these regions over equatorial latitudes have been only reliably measured by a few in situ rocket probes [e.g., *Pfaff et al.*, 1987; *Friedrich and Torkar*, 2001].

[3] The main obstacles at Jicamarca to previously performing these measurements have been mainly due to the occurrence of strong coherent scatter echoes from equatorial electrojet (EEJ) irregularities and mesospheric turbulent layers. Briefly, coherent EEJ echoes are present most of the time during the day, are very strong (~40–70 dB stronger than ISR echoes), and they arrive from the 95–110 km region [e.g., *Farley*, 1985]. We should recall that the ISR technique works only when the medium is in quasi-thermodynamic equilibrium, i.e., when nonthermal fluctuations are absent. Coherent echoes from mesospheric layers are also very strong (10–20 dB stronger than ISR echoes at similar altitudes), are organized in thin layers, occur during the day, and occupy the 60–90 km altitudinal region [e.g., *Woodman and Guillén*, 1974; *Kudeki*, 1988; *Woodman*, 1994; *Lehmacher and Kudeki*, 2003].

[4] The measurements presented here have been performed using a high-resolution Faraday rotation experiment (see section 2 for details). In the case of the electron densities around the *E* peak, they have been possible due to the fortuitous occurrence of a weak EEJ event (i.e., almost zero horizontal electric field) while we were observing, which inhibited the occurrence of coherent EEJ echoes. Measurements of the *D* and upper *E* region are mainly possible due to the recent improvements on the acquisition and receiving systems at Jicamarca that allow higher range resolution and higher dynamic range than before.

[5] We compare our results with values obtained from the following:

[6] 1. A digisonde portable system (DPS) that measures the *F* and *E* region peak densities and altitudes. In addition, the DPS provides fitted bottomside profiles and inferred topside densities [*Reinisch*, 1986].

[7] 2. The International Reference Ionosphere (IRI) empirical model. For a given location, time, and date, IRI provides electron densities from 60 (80) km during the day (night) up to 2000 km [e.g., *Bilitza*, 2001].

[8] 3. The FIRI model. FIRI is an option of IRI for the *D* and *E* region, but using electron density data based on Faraday rotation experiments conducted on flying rockets.

0148-0227/05/2005JA011438$09.00

FIRI provides electron densities between 60 and 140 km [*Friedrich and Torkar*, 2001].

[9] 4. The Danilov's model. This model is an option provided by IRI model for the *D* region (below 90 km). More details are given by *Danilov* [2000].

[10] The paper is organized as follows. First, we describe the experimental setup and present some useful radar expressions we need to explain and discuss the results. Then we discuss separately the *E* and *D* region results and present our conclusions.

2. Experimental Setup

[11] The observations reported in this work have been made with a high-resolution Faraday rotation experiment to get absolute electron densities between ~130 and 400 km altitude. Faraday rotation experiments have been conducted at Jicamarca since the early 1960s [e.g., *Farley*, 1969a]. Briefly, Faraday rotation arises from the difference between the indices of refraction corresponding to the two characteristic modes of a magnetoionic medium. Since the operating frequency at JRO (50 MHz) is much greater than the electron gyrofrequency, the quasi-longitudinal (QL) approximation of the magnetoionic theory [*Ratcliffe*, 1959] is valid even when the radar beam is directed nearly perpendicular to the magnetic field. To be more specific, the QL approximation is valid at Jicamarca as long as the angle between the magnetic field (**B**) and the wave vector (*k*) is somewhat less than 89.6° [*Farley*, 1969a]. In order to increase the sensitivity of the system, we have used JRO's on-axis antenna position (~88.17° at the epoch the experiment was performed); therefore the two characteristic waves are right and left circularly polarized.

[12] The experiment consisted on transmitting each of the circular polarizations with an independent ~1 MW (peak power) transmitter (A and B). The major cross-talk effects have been removed using a 180° phase shift to every other pulse of one of the polarizations (in this case B) [*Farley*, 1969a]. On reception, circular polarizations are synthesized in hardware (using 0–180° hybrids) from linear polarizations. The circularly polarized signals are then received and processed by a digital receiver system. Using the digital receivers, many of the instrumental error corrections performed in previous Faraday rotation experiments, for example, in-phase and quadrature imperfections, are no longer needed. Moreover, the current digital receiver system allows better throughput and larger dynamic range (16 bits instead of 8 bits) compared to the previous analog system. More details of the standard Faraday rotation experiments are given by *Pingree* [1990].

[13] As mentioned in section 1, the main purpose of this experiment was to improved the altitudinal resolution of the density estimates below 200 km. Therefore compared to a standard Faraday rotation experiment, we have used shorter coded pulses and avoid using delayed double pulses. Double pulses are used in order to estimate the ISR autocorrelation function (ACF) but at the expense of not using the available duty cycle [*Farley*, 1969a].

[14] The main parameters of our experiment are presented in Table 1. We have used the full duty cycle available (5%) and a reasonably high range resolution by using a 28-bit binary code [*Gray and Farley*, 1973] with 0.75 km baud width.

Table 1. Radar Parameters for Faraday Rotation Experiments on 13 December 2004

Parameter	Value	Units
Inter pulse period (IPP)	420	km
Pulse width	21	km
Binary code	28	bits
Receiver Bandwidth	5	μs
Sampling rate	5 (0.75)	μs (km)
Initial range	50	km
Number of samples	456	
Number of complex channels	2	
Transmitter peak power	2	MW

3. Radar Expressions

[15] In this section we summarize some of the useful radar expressions that are needed to derived the *D* and *E* region density measurements at Jicamarca from ISR power measurements.

[16] Absolute ISR radar measurements can be obtained from the radar equation of a soft target if a system constant (K_s) is known [e.g., *Bowles et al.*, 1962]. However, getting such a constant requires measurements that were not available at the time of the experiment (e.g., transmitter power, receiver gains, etc.).

[17] It is well known that the received ISR power (P_s) is proportional to the electron density (N_e), $1/h^2$ (h is the altitude of the scattering volume), and the normalized scattering cross-section of electrons (σ_{ne}), i.e.,

$$P_s(h) = K_s N_e(h) \sigma_{ne}(h)/h^2. \tag{1}$$

[18] The normalized scattering cross-section of electrons is a function of the T_e/T_i ratio [*Farley*, 1966]. In the case of our observations, i.e., pointing angles away from perpendicular to **B**, radar Bragg wavelength (3 m) much greater than the Debye length, $1 \leq T_e/T_i \leq 3$, and no negative ions, σ_{ne} is given by,

$$\sigma_{ne} = r_e^2 \frac{1}{1 + T_e/T_i}, \tag{2}$$

where r_e is the electron radius.

[19] In the *D* region, T_e/T_i is usually assumed to be equal to 1 [*Mathews*, 1986]; however, σ_{ne} becomes a function of negative ion composition [*Mathews*, 1978], as follows:

$$\sigma_{ne} = r_e^2 \frac{1 + \alpha_e^{-2}(1 + 2\lambda_-)}{1 + 2\alpha_e^{-2}(1 + \lambda_-)}, \tag{3}$$

where $\lambda_- = N_-/N_e$, N_- is the total concentration of negative ions, $\alpha_e = 4\pi\lambda_D/\lambda_0$, λ_D is the Debye length, and λ_0 the radar wavelength. In this paper we are assuming there are no negative ions at the altitudes of interest (see section 4 for details). At *D* region altitudes this assumption could be questioned. However, if λ_- was known to be otherwise, the actual electron density values could be obtained with the use of (3). In any case the correction is small, less than the uncertainty of our results.

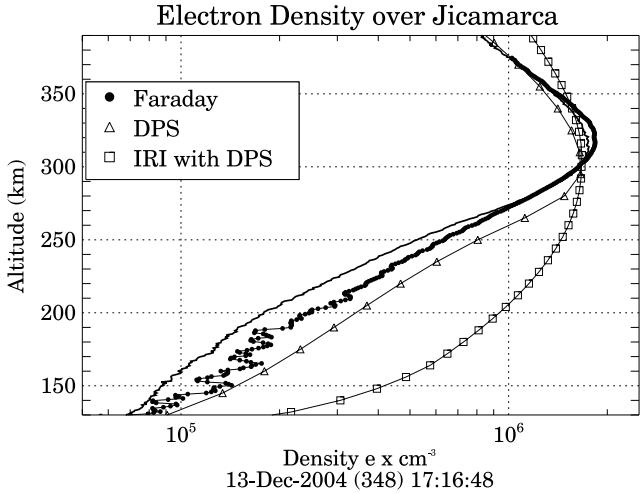

Figure 1. *F* region electron density profiles over Jicamarca obtained on 13 December 2004 around 1700 LT: (a) ISR power in density units (solid line), ISR densities from Faraday rotation measurements (filled circle), inferred ionosonde profiles (triangle), and IRI values (square).

[20] Since power measurements are obtained from averaging power signals from different radar pulses, the resultant signal error level (assuming stationarity) is [e.g., *Farley*, 1969b]

$$\frac{\Delta P_s}{P_s} = \frac{1 + P_n/P_s}{\sqrt{N}}, \tag{4}$$

where ΔP_s is one standard deviation, P_n is the noise power, and N is the number of independent samples.

[21] As mentioned in the previous section, electron density profiles are also possible from Faraday rotation experiments, by measuring the phase shift between received circularly polarized signals. N_e is related to this phase shift by

$$N_e(h) = K_f d\phi/dh, \tag{5}$$

where the factor K_f is proportional to f^2 B cos α, f is the radar frequency, B is the magnetic field strength, and α is the angle of the radar beam with respect to **B**. This angle and the magnitude of **B** are reliably obtained from the International Geomagnetic Reference Field (IGRF) 2000 magnetic field model [*Barton*, 1997]. Note that the density measurements from Faraday rotation are not dependent on either the T_e/T_i ratio or the presence of negative ions, and besides, given absolute density measurements, it can be used to find the system constant (K_s) in (1), e.g., at altitudes where $T_e = T_i$.

4. Electron Density Measurements

[22] In this section we present the main results of this work, i.e., the *E* and *D* region ISR densities. However, we first start with the presentation of the *F* region density measurements that are needed to calibrate the *D* and *E* region observations.

[23] Figure 1 shows the normalized ISR power profiles (between 130 and 390 km) in electron density units (solid lines). These values have been obtained finding the K_s factor needed in (1) to minimize the difference between the Faraday profile (filled circles) and the density from power around the *F* region peak (F_{peak}). In this region T_e/T_i is known to be 1 [e.g., [*Farley et al.*, 1967]]. Previously, noise estimates obtained from lower altitudes have been removed from the total power measurements and the resulting value corrected by the h^2 dependence. The agreement between these two radar estimates of N_e is excellent. Differences between 130 and 260 km are due to $T_e/T_i > 1$ for this time of the day at those altitudes [e.g., *Farley et al.*, 1967], causing the uncorrected densities (from power) to be less than the densities from Faraday rotation (see (1) and (2)).

[24] In addition, we compare the radar measurements with the density profile inferred from the Jicamarca DPS (triangle), and IRI model values (square) for conditions appropriate for the time of the comparison. There is good agreement with the DPS values, the small discrepancies might be due to the different instrumental resolutions being compared. Below the *F* peak, the ionosonde slightly overestimates the Faraday densities. The IRI profiles show a poor agreement with ISR and DPS values, particularly below the F_{peak}.

[25] Once the *F* region ISR power have been calibrated, we extended the calibration to the lower altitudes. In Figure 2a we show the power profiles in density units below 150 km. Owing to collisions, the ISR spectrum narrows considerably below 110 km [*Dougherty and Farley*, 1963]. This allow us to use coherent integration (ncoh) to improve the signal to noise ratio (SNR). Between 80 and 95 km, we have used ncoh = 8 (diamond), while below 80 km ncoh = 32 (square). The enhancements below 95 km are due to coherent scatter echoes from narrow turbulent layers [e.g., *Woodman and Guillén*, 1974]. The solid circles represent the assumed ISR levels. The unfilled squares, with power levels above the minimum values, are taken to be enhanced (coherent) by turbulence and excluded from the profile. Note the strong coherent echo between 85 and 90 km altitudes, probably due to turbulence. Normally, turbulent echo observations stop at 85 km because electrodynamic considerations (enhancements and drifts) complicate their interpretation. However, in this case the electric field is zero.

[26] Now in Figure 2b we show the 15-min averaged ISR power profile (in density units) against density profiles from DPS, FIRI, IRI, and Danilov's model. Note that there is an excellent agreement above 90 km with FIRI values which are based on rocket measurements. There is also a good agreement with IRI and DPS *E* region peak values. However, IRI overestimates the bottom *E* region profiles. This latter result is in agreement with the findings of *Shume et al.* [2005].

[27] The *D* region ISR densities, i.e., below 90 km, are larger than the values given by all three model estimates above 70 km, i.e., IRI, FIRI, and Danilov's. Below 70 km, they are in reasonable agreement with extrapolated FIRI values (see section 5 for details).

5. Discussion

[28] In the previous section we have already discussed some of the results, particularly the comparisons around the

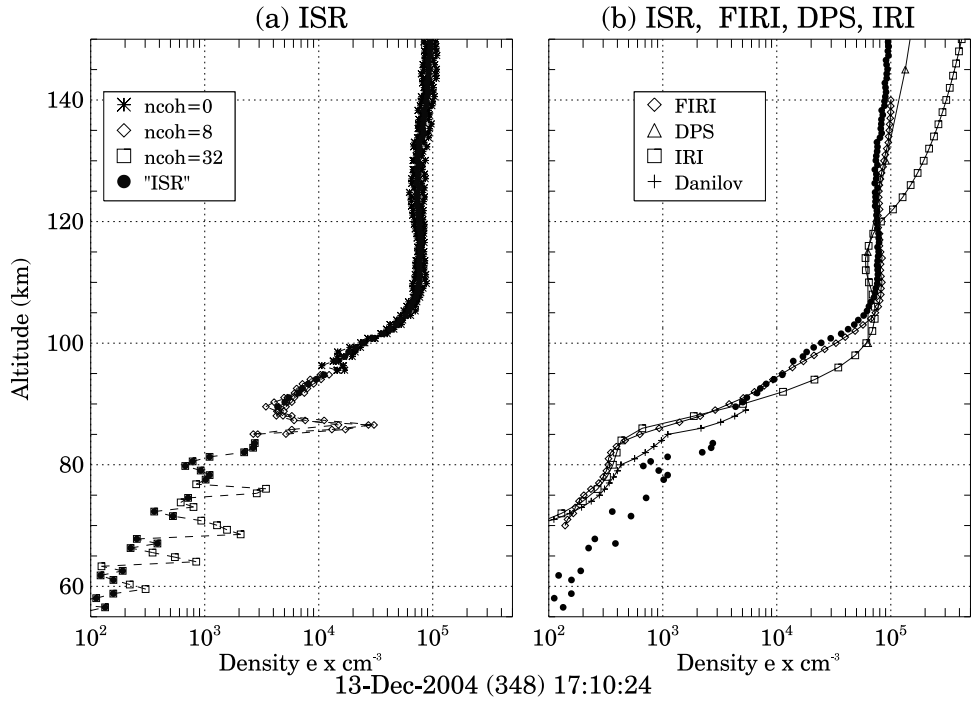

Figure 2. *E* and *D* region electron density profiles. (a) Power measurements in density units using 0 (asterisk), 8 (diamond), and 32 (square) coherent integrations. The ISR densities (after removing the coherent echoes) are shown with black dots (filled circle). (b) Comparisons of radar density estimates with FIRI (diamond), DPS (triangle), IRI (square), and Danilov's model (plus symbol).

F peak. In this section we concentrate our discussions on the (1) *E* region and (2) *D* region ISR densities.

5.1. *E* Region ISR Densities

[29] As mentioned in the Introduction, this is the first time *E* region densities are directly measured over Jicamarca, thanks to the absence of strong EEJ echoes that normally preclude those measurements. Typical daytime EEJ irregularities occur between ~95 and 110 km [e.g., *Farley*, 1985]; therefore ISR measurements are precluded around that altitudinal region. The extension of the affected region will depend on the effective pulse width of the experiment. In the past, ISR measurements at Jicamarca were performed with relatively long pulses (50 μs to 300 μs), extending the EEJ clutter to higher altitudes. At times the EEJ echoes were so strong that echoes coming from antenna side lobes cluttered even higher altitude range.

[30] Our results are in excellent agreement with an empirical model based on rocket measurements (FIRI). It is important to note that this capability will only work during the daytime during weak EEJ events. At night, the *E* region density is known to have significant structure, so that EEJ coherent echoes will be always present. Recently, *Hysell and Chau* [2001] have developed a technique that uses a bistatic system to get *E* region density profiles from signals scattered from the strong EEJ irregularities. These results have been successfully compared with other techniques by *Shume et al.* [2005] and our results are in very good agreement with theirs.

[31] Another important contribution from the high resolution mode we have implemented is the possibility of getting high resolution density measurements between 120 and 200 km from Faraday rotation measurements. Since this mode uses relative short pulses, the EEJ clutter, even if it is strong, is confined to few altitudinal ranges around 100–110 km. In fact, we have already used this mode to study the electron density between 130 and 180 km, where the so-called 150-km echoes occur [e.g., *Kudeki and Fawcett*, 1993; *Chau*, 2004]. Note that current IRI model significantly overestimates the densities below the *F* peak.

5.2. *D* Region ISR Densities

[32] ISR *D* region observations have not been performed before at equatorial latitudes. At Jicamarca, given its frequency (the lowest of the ISR chain), it is particularly difficult to perform these measurements due to the presence of coherent echoes from mesospheric turbulent layers. Moreover, the presence of the strong EEJ echoes precludes the use of very long pulses used at other sites [e.g., *Mathews*, 1986, and references therein]. However, fortunately, the turbulent layers are usually organized in very narrow layers [e.g., *Kudeki*, 1988; *Woodman*, 1994; *Lehmacher and Kudeki*, 2003]. We have taken advantage of this, to get ISR densities from the "unperturbed" regions in between.

[33] Although the ISR spectra information is not a subject of this work, in Figure 3 we show a spectrogram of the radar signals obtained between 60 and 100 km after 32 coherent integrations and 15-min averaging, to give the reader confidence on the *D* region information we are presenting. There is a slight contribution from range aliased ISR signal from the altitudes above 420 km (our IPP). Fortunately, the *F* region spectra have very wide thermal widths and thus, when aliased, appear as a featureless base level (like

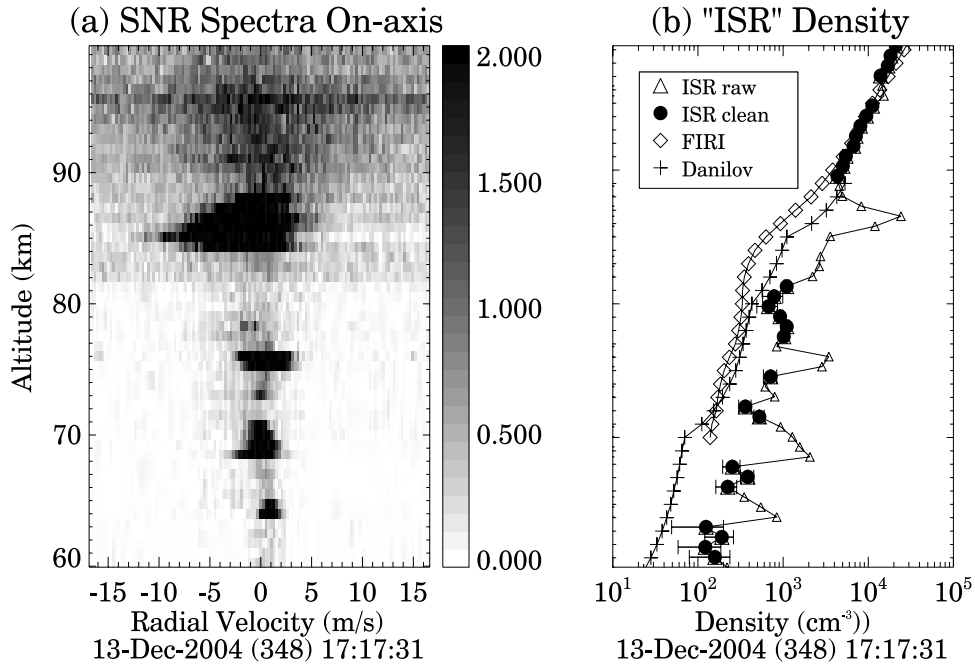

Figure 3. (a) Spectrogram obtained from pulse-to-pulse analysis between 60 and 100 km after 32 coherent integrations and incoherently averaged for 15 min. (b) Profiles of power profiles in density units before (triangle) and after (filled circle) removing coherent echoes; electron densities from FIRI (diamond) and Danilov's (plus symbol).

''white'' noise). The ratio of *D* power to *F* (aliased) power after coherent integration is 0.5–0.1 between 60 and 85 km s.

[34] We can note that the spectra gets narrower as the altitude gets lower, as expected. Typical spectral widths correspond to 1–5 seconds of correlation time. These correlation times are shorter than what we expect from a collision dominated ISR spectra at these altitudes, using temperatures and collision frequencies derived from the Mass Spectrometer Incoherent Scatter Model (MSIS) [e.g., *Hedin*, 1991]. For example, at 70 km, we expected a correlation time of 10 s, and we measured 6 s (i.e., a wider spectral width). We attribute such shorter times (wider spectral widths) to Doppler broadening due to gravity waves, that are known to affect spectral width measurements in this region [e.g., *Hocking*, 1996]. More details on the spectra characteristics of this region are presented by J. L. Chau and E. Kudeki (First *E* and *D* region incoherent scatter spectra observed over Jicamarca, submitted to *Annales Geophysicae*, 2005).

[35] In addition, in Figure 3, we present their corresponding ISR power profiles in density units (filled circle). The points labeled with a triangle symbol are assumed to be enhanced coherent echoes. This editing procedure have been based on the larger signal strength and spectral width, than expected from a medium in thermal equilibrium. We also show the expected statistical uncertainties for the edited values. We can see that the resulting ISR densities are slightly larger than the values given by the models (FIRI and Danilov's) above 70 km but are in reasonable agreement (within the statistical uncertainties) with extrapolated values from FIRI, below 70 km.

[36] In a previous section we have pointed out the possible effects of negative ions on the measured ISR power, but recent theoretical models suggest that negative ions are expected to disappear above 60 km [e.g., *Kazil et al.*, 2003]. Moreover, measurements performed by rocket-borne mass spectrometers have shown that daytime negative ions were only detected at very low heights (<60 km) where the reliability of the measurements is poor (M. Friedrich, personal communication, 2005). Nonetheless, we have performed the correction of negative ions as suggested by *Mathews et al.* [1982], but the correction is at most a factor of 2 lower values (results not shown here).

[37] Our claim that the minimum power profile is a measure of electron density is based on one single assumption: that turbulence at these altitudes is intermittent, i.e., it occurs in layers of finite temporal duration with quiet regions in between. It has been proposed that horizontally extended regions with sharp vertical gradients in density could also produce enhanced echoes through a partial (Fresnel) reflection mechanism [e.g., *Röttger*, 1980]. Chances are that such gradients are also a consequence of turbulence [e.g., *Bolgiano*, 1968; *Woodman and Chu*, 1989]. In any case, they are also intermittent in altitude and time. Outside these regions the medium would be in thermodynamic equilibrium and its density fluctuation would be at a minimum level as predicted by IS theories. The intermittent nature of turbulence is an experimental fact [e.g., *Woodman*, 1994; *Kudeki*, 1988] to be expected on theoretical grounds for a region where the shears vary in altitude in a sinusoidal fashion as a superposition of waves of different wave length. Such conditions, in a region of either constant or varying temperature gradients, would

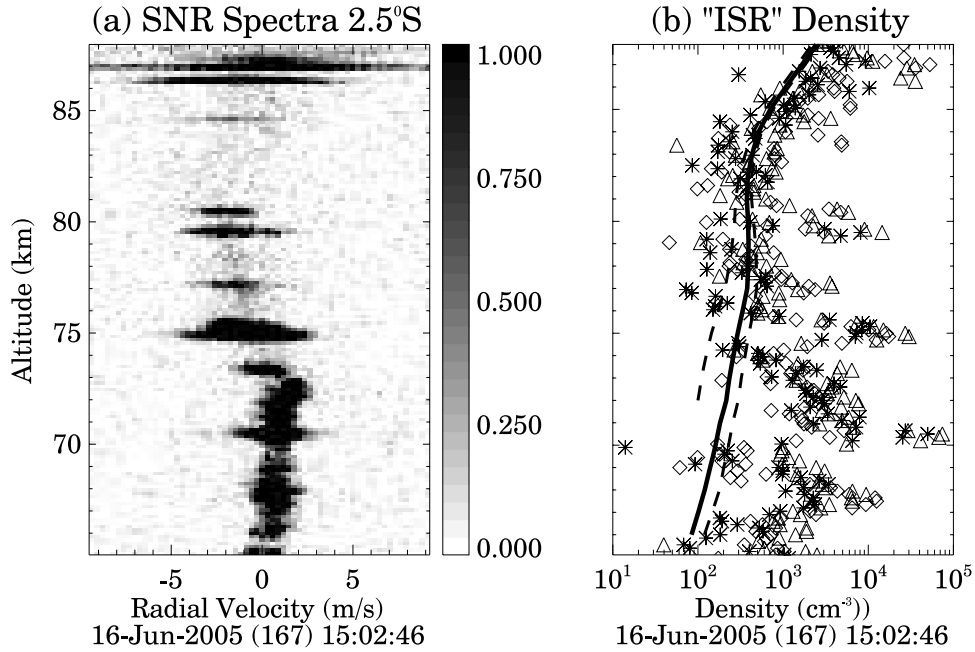

Figure 4. (a) Spectrogram obtained from pulse-to-pulse analysis between 60 and 88 km incoherently averaged for 30 min for antenna pointing 2.5°S, and (b) power profiles in density units for four different antennas (different symbols). The corresponding FIRI profile is shown in solid line, while profiles for one hour after and before are shown in dashed lines. Power measurements much larger than the FIRI profiles represent the coherent echoes (black regions in Figure 4a).

produce a profile of varying Richardson numbers with only occasional regions where it goes unstable ($R_i \leq 0.25$). It would be certainly stable when the shear approaches or crosses zero in its sinusoidal variations.

[38] The results presented above are in reasonable agreement with models below 70 km and slightly large between 70 and 90 km; however, in Figure 4 we show another example taken from a recent campaign to provide further support to our technique. Briefly, these new results have been obtained with a less sensitive mode (note the scale of SNR) than what we have used. Namely, the whole antenna was split in four smaller antennas each pointing in different direction (2.5° from vertical in north, east, west, and south directions) and using a range resolution 1/5 of what we have used, i.e., 1 μs (details of the experimental setup are shown by R. Sheth et al. (A high-resolution study of mesospheric fine structure with the Jicamarca MST radar, submitted to *Annales Geophysicae*, 2005)). In the left panel we show the spectra of one of the antenna positions (2.5°S) after 30 min of integration. The right panel shows the 30-min power profiles in density units from all four antenna positions used.

[39] For comparison we show the FIRI profiles for the time of the experiment in solid line. The dashed line on the right (left) shows the FIRI values for 1 hour before (after). Although we are not showing the statistical uncertainties of the estimates to avoid cluttering the figure, it is clear that densities associated with the gaps in the spectra (regions of less power but above noise and narrow spectral width) are in very good agreement with the empirical FIRI values. We think the better agreement of the less sensitive mode compared to results of Figure 3 are due to the higher resolution used. Having a higher range resolution provides better chances of catching the stable gaps. The poorer the range resolution, the greater the chances of getting mixed stable and unstable regions. Higher resolution experiments are less sensitive and therefore more integration time is required to produce reasonable values.

[40] Given our encouraging results, we plan to perform the *D* region analysis at different times of the days and seasons, to get their diurnal and seasonal characteristics. Moreover, these type of measurements will also allow the measurements of accurate wind velocities. So far, mesospheric velocities have been obtained only from the coherent echoes [e.g., *Woodman and Guillén*, 1974], we expect the velocities from the weak ISR mesospheric echoes to fill the gaps in this region, although after a longer integration time (30 min compared to 1–5 min). Note that these measurements are only possible during the day, at night there is no sufficient electron density to get echoes.

6. Conclusions

[41] The main contributions of this work can be divided into (1) *E* region and (2) *D* region ISR densities. We have reported the first daytime *E* region ISR density profiles measured directly with the Jicamarca radar. These measurements have been possible during a weak EEJ event when the usual strong coherent echoes from EEJ irregularities do not clutter the ISR observations. Moreover, they show an excellent agreement with empirical model based on rocket measurements, i.e., FIRI.

[42] Although weak EEJ events are not common, we have shown that the observations are easy to perform, and we plan to add this mode to Jicamarca standard ISR operations to make similar observations when those events occur.

Moreover, this mode is also suitable to measure densities between 130 and 200 km even during strong EEJ events using Faraday rotation. We are currently using these measurements to study the density profiles associated with the so-called 150-km echoes.

[43] We also report the first daytime *D* region ISR density profiles measured at Jicamarca. We have been able to perform these measurements using high range resolutions, which allow us to get measurements between the strong mesospheric coherent echoes usually organized in narrow separated layers. Preliminary comparisons with empirical *D* region models show that our results are in reasonable agreement with empirical models. There is no way that larger electron densities would produce power levels lower than what IS would predict. An upper limit this close becomes important in the *D* region, where the physical and chemical processes responsible for the ionization level is not well understood. The importance of our observations would be even greater if our assumption is correct. We should get more confidence in the validity of this assumption if future observations show consistency in the results.

[44] **Acknowledgments.** We thank M. Friedrich for sharing with us the FIRI model and profiles, and fruitful discussions with E. Kudeki and G. Lehmacher. We also thank the Jicamarca staff for performing the experiments, in particular P. Reyes and R. Ilma. The IRI and MSIS results were obtained from the web pages of NASA's National Space Science Data Center. The Jicamarca Radio Observatory is a facility of the Instituto Geofísico del Perú and is operated with support from the NSF Cooperative Agreement ATM-0432565 through Cornell University.

[45] Arthur Richmond thanks Martin Friedrich and David Hysell for their assistance in evaluating this paper.

References

Barton, C. E. (1997), International geomagnetic reference field: The seventh generation, *J. Geomagn. Geoelectr.*, *49*, 123.

Bilitza, D. (2001), International reference ionosphere 2000, *Radio Sci.*, *36*, 261.

Bolgiano, R. (1968), The general theory of turbulence: Turbulence in the atmosphere, in *Wind and Turbulence in the Stratosphere, Mesosphere and Ionosphere*, edited by K. Rawer, pp. 371–400, North-Holland, New York.

Bowles, K. L., G. R. Ochs, and J. L. Green (1962), On the absolute intensity of incoherent scatter echoes from the ionosphere, *J. Res. NBS*, *66D*, 395–407.

Chau, J. L. (2004), Unexpected spectral characteristics of VHF radar signals from 150-km region over Jicamarca, *Geophys. Res. Lett.*, *31*, L23803, doi:10.1029/2004GL021620.

Danilov, A. D. (2000), New ideas on the *D*-region modeling, *Adv. Space Res.*, *25*, 5–14.

Dougherty, J. P., and D. T. Farley (1963), A theory of incoherent scattering of radio waves by a plasma, *J. Geophys. Res.*, *68*, 5473–5486.

Farley, D. T. (1966), A theory of incoherent scattering of radio waves by a plasma, 4, The effect of unequal ion and electron temperatures, *J. Geophys. Res.*, *71*, 4091.

Farley, D. T. (1969a), Faraday rotation measurements using incoherent scatter, *Radio Sci.*, *4*, 143–152.

Farley, D. T. (1969b), Incoherent scatter power measurements: A comparison of various techniques, *Radio Sci.*, *4*, 139–142.

Farley, D. T. (1985), Theory of equatorial electrojet plasma waves: New developments and current status, *J. Atmos. Sol. Terr. Phys.*, *47*, 729–744.

Farley, D., J. P. McClure, D. L. Sterling, and J. L. Green (1967), Temperatures and composition of the equatorial ionosphere, *J. Geophys. Res.*, *72*, 5837–5851.

Friedrich, M., and K. M. Torkar (2001), FIRI: A simiempirical model of the lower ionosphere, *J. Geophys. Res.*, *106*, 21,409–21,418.

Gray, R. W., and D. T. Farley (1973), Theory of incoherent-scatter measurements using compressed pulses, *Radio Sci.*, *8*, 123.

Hedin, A. E. (1991), Extension of the MSIS thermospheric model into the middle and lower atmosphere, *J. Geophys. Res.*, *96*, 1159.

Hocking, W. K. (1996), An assessment of the capabilities and limitations of radars in measurements of upper atmosphere turbulence, *Adv. Space Res.*, *17*, 37–47.

Hysell, D. L., and J. L. Chau (2001), Inferring *E* region electron density profiles at Jicamarca from Faraday rotation of coherent scatter, *J. Geophys. Res.*, *106*, 30,371.

Kazil, J., E. Kopp, S. Chabrillat, and J. Bishop (2003), The University of Bern atmospheric ion model: Time dependent ions modeling in the mesosphere and lower thermosphere, *J. Geophys. Res.*, *108*(D14), 4432, doi:10.1029/2002JD003024.

Kudeki, E. (1988), Radar interferometer observations of mesospheric echoing layers at Jicamarca, *J. Geophys. Res.*, *93*, 5413–5421.

Kudeki, E., and C. D. Fawcett (1993), High resolution observations of 150 km echoes at Jicamarca, *Geophys. Res. Lett.*, *20*, 1987–1990.

Lehmacher, G., and E. Kudeki (2003), Variability of equatorial mesospheric echoes, *Adv. Space Res.*, *32*, 747–752.

Mathews, J. D. (1978), The effects of negative ions on coliision-dominated Thomson scattering, *J. Geophys. Res.*, *83*, 505–512.

Mathews, J. D. (1986), Incoherent scatter radar probing of the 60–100-km atmosphere and ionosphere, *IEEE Trans. Geosci. Remote Sens.*, *24*, 765–776.

Mathews, J. D., J. K. Breakall, and S. Ganguly (1982), The measurements of diurnal variations of electron concentration in the 60–100 km ionosphere at Arecibo, *J. Atmos. Sol. Terr. Phys.*, *44*, 441–448.

Pfaff, R. F., M. C. Kelley, E. Kudeki, B. G. Fejer, and K. D. Baker (1987), Electric field and plasma density measurements in the strongly driven daytime equatorial electrojet, 1, The unstable layer and gradient drift waves, *J. Geophys. Res.*, *92*, 13,578.

Pingree, J. E. (1990), Incoherent scatter measurements and inferred energy fluxes in the equarotial *F*-region ionosphere, Ph.D. thesis, Cornell Univ., Ithaca, N. Y.

Ratcliffe, J. A. (1959), *The Magnetoionic Theory and Ist Applications to the Ionosphere*, Cambridge Univ. Press, New York.

Reinisch, B. W. (1986), New techniques in groud-based ionospheric sounding and studies, *Radio Sci.*, *21*, 331–341.

Röttger, J. (1980), Reflection and scattering of VHF radar signals from atmospheric refractivity structures, *Radio Sci.*, *15*, 259–276.

Shume, E. B., D. L. Hysell, and J. L. Chau (2005), Electron density profiles in the equatorial *E* region ionosphere derived from a bistatic coherent scatter radar experiment in Peru, *Geophys. Res. Lett.*, *32*, L01107, doi:10.1029/2004GL021715.

Woodman, R. (1994), Equatorial ionospheric irregularities as observed by the Jicamarca radar, in *Low-Latitude Ionospheric Physics: Proceedings of COSPAR Colloquium on Low-Latitude Ionospheric Physics*, edited by F.-S. Kuo, pp. 83–95, Elsevier, New York.

Woodman, R. F., and Y. Y.-H. Chu (1989), Aspect sensitivity measurements of VHF backscatter made with the Chung-Li radar: Plausible mechanisms, *Radio Sci.*, *24*, 113–126.

Woodman, R. F., and A. Guillén (1974), Radar observations of winds and turbulence in the stratosphere and mesosphere, *J. Atmos. Sci.*, *31*, 493–505.

J. L. Chau and R. F. Woodman, Radio Observatorio de Jicamarca, Apartado 13-0207, Lima 13, Perú. (jchau@jro.igp.gob.pe; ronw@geo.igp.gob.pe)